AFS Proceedings 2012 © American Foundry Society, Schaumburg, IL USA

Measurements and Confirmation of Thermal Properties of Investment Ceramic Shell by Multiple Methods

M. Xu, S.N. Lekakh, C. Mahimkar, V.L. Richards
Missouri University of Science and Technology, Rolla, Missouri

S.A. Dutler
MAGMA Foundry Technologies, Inc., Schaumburg, Illinois

ABSTRACT

Prediction of solidification shrinkage during investment casting requires applicable and realistic thermal properties of the ceramic shell. The objective of this research was to study the thermal properties of ceramic investment casting shells using different measurement methods and to evaluate the applicability of this data for the modeling of the investment casting process using casting process simulation software. Thermal properties of an industrial shell were investigated using the Laser Flash method and compared to previous Differential Scanning Calorimetry (DSC) results. In addition, to assess the properties determined by these physical methods, inverse modeling of experimental cooling curves was performed. A melt with known properties (pure Ni) was poured into the ceramic shell molds which had thermocouples located in the center of casting and outside the shell layer. Inverse modeling using the proprietary casting process simulation software, Magmasoft® and its additional optimization tool were applied to calculate temperature dependent heat capacity and thermal conductivity of the shell. The effects of the shell microstructure and porosity on thermal properties are discussed. A modified laser flash procedure is presented which minimizes the influence of open pores at the surface. The experimental/modeling data were compared to theoretically predicted data. The results obtained will be used for improving the precision of investment casting process modeling.

Keywords: ceramic shell, investment casting, thermal properties.

INTRODUCTION

Steel casting solidification significantly differs in relatively thin (5-15 mm [0.20-0.59 in.] thickness) ceramic shells when compared to more massive sand molds. A typical sand mold can be considered as a semi-infinite cooling medium during casting solidification. In the investment casting shell, two different heat transfer scenarios are possible, depending on casting-to-shell wall thickness ratio: i) most of the melt superheat and latent heat are accumulated by the shell and shell enthalpy plays a major role in thin-walled casting solidification and ii) a significant part of latent heat transfers through the shell to the environment so that shell thermal conductivity controls solidification in the case of relatively thick-walled casting.

Considering that a variety of ceramic shell compositions and processing parameters are currently available, the investment casting process allows providing a desired and controllable solidification mode, including cooling rate and thermal gradient. It is important to note that the ceramic shell could be considered as a material with moderate porosity (10-30%) having some volume fraction of open interconnected porosity which provides air permeability.[1, 2] The variation in levels of porosity strongly affects mechanical and thermal properties of ceramic molds.[3-5] The porosity of an investment casting shell depends on shell formulation, processing and thermal history. Moreover, shell porosity can be specifically engineered such as applying sacrificial additions like graphite particles.[6] Variations in slurry viscosity, stucco particle size and method of stuccoing (rain fall versus fluidized bed) can develop monolithic or layered shell structure[7] which influences shell porosity and properties.

Another important factor is shell processing thermal history. Typically shells are exposed to high temperature during pattern removal, sintering/burnout and preheating before pouring. Considering that colloidal silica binder as well as filler and often stucco ceramics are amorphous silica to a significant extent, the degree to which the amorphous to crystalline transformation, which takes place during high temperature processing,[8] can also affect the thermal properties of the shell.

Generally speaking, three main approaches can be used for evaluation of ceramic shell thermal properties. The first approach can be estimation based on tabulated thermal properties of pure monolithic oxides and the rule of mixtures. The high porosity of a real investment casting ceramic mold shell provides significantly different properties when compared to a monolithic ceramic. Equation1 was proposed for estimating thermal conductivity of porous materials.[5]

$$k_r = exp(-1.5\,\phi/(1-\phi)) \qquad \text{Equation 1}$$

where: ϕ is the porosity and $k_r = k/k_0$ is the relative thermal conductivity, with k denoting the effective thermal conductivity of the porous material and k_0 denoting the thermal conductivity of the solid phase.

In the second approach, different physical methods are used for experimental measurements. In laser flash method, a homogenized laser beam as heating source for front surface and infrared thermometer to measure temperature response on back surface is used for determination of shell properties.[4, 9] The main problem with this approach follows from using a small specimen size (2 mm [0.08 in.] thick disc) while shells are non-homogeneous on a relatively large scale. Large pores in the shell, sized on the order of 100µm, can produce measurement distortions. For example, pores at the surface of specimen would significantly reduce effective thickness. To counter this distortion, Garcia[10] suggested attaching two thin copper disks to a porous specimen to ensure a known effective thickness. However this method is not applicable for a brittle investment ceramic shell.

Connolly et al[9] measured the specific heat capacity of investment casting shells prepared from a slurry consisting of a 3.7:1 (by weight) mixture of zircon and silica in an aqueous colloidal silica solution. Huang et al.[11] measured thermal conductivity of investment casting ceramics using hot wire method, but they obtained the data for pure materials used in investment casting processing and not the composite shell structure. Most of the work done so far is limited to temperatures about 800C (1472F) or less due to difficulties in measurement at higher temperatures. Also, porosity in the shell structure accounts for the considerable variation in the measurement.

In the third approach, the "inverse method" which characterizes the thermal properties of the entire shell is used. In this case, a shell with installed thermocouples is poured with a pure liquid metal which has well defined properties. Shell thermal properties are estimated by running multiple computational fluid dynamic (CFD) simulation iterations varying the thermal conductivity and specific heat capacity over a range of different values in an effort to fit the calculated cooling curves to the experimental cooling curves for the shell and alloy.[12] Sabau and Viswanathan[13] studied thermo-physical properties of zircon and fused silica based investment casting shells using the "inverse method." They measured thermal diffusivity (a) of zircon based prime coat and generated C_p and coefficient of thermal conductivity (K) data from it.

In this paper, the determination of temperature-dependent thermal properties of industrially produced investment mold shells was done based on combination of different experimental and modeling approaches, including direct laboratory measurements of thermal properties and application of "inverse method" CFD analysis to experimentally generated cooling curves. High purity nickel was used as the metal of known properties with which to pour the test castings.

PROCEDURES

THERMAL PROPERTIES MEASUREMENTS

In a laser flash thermal diffusivity test, a small specimen is subjected to high intensity short duration radiant laser pulses. Typical specimen disc dimensions are 12.7 mm (0.5 in.) diameter by 2 mm (0.08 in.) thickness. To insure similar emissivity, the front and rear faces of both the reference and the test specimens are covered with graphite spray coating. The energy of the pulse is absorbed on the front surface of the specimen and the resulting rear face temperature rise is recorded. The thermal diffusivity value (α) is calculated[14] from specimen thickness (L) and time ($t_{1/2}$) required for rear face temperature to reach 50% of its maximal value (Equation 2):

$$\alpha = 0.1388L^2/t_{1/2} \qquad \text{Equation 2}$$

In differential laser flash calorimetry, a reference specimen (subscript "R") and the test specimen (subscript "M"), are mounted together under the same condition at the same temperature and irradiated uniformly with homogenized laser beam. The temperature rise (ΔT) of the reference (graphite) with known specific heat capacity (C_p) and the specimen (shell) are measured with non-contact infrared radiation thermometer. If the density (ρ) of the shell is known then specific heat capacity of the shell can be calculated (Equation 3):

$$\left(\rho c_p\right)_M = \frac{L_R \Delta T_R}{L_M \Delta T_M}\left(\rho c_p\right)_R \qquad \text{Equation 3}$$

Finally, thermal conductivity (K) of the shell can be calculated by substituting measured value of specific heat capacity along with the thermal diffusivity in (Equation 4):

$$K = \rho C_p \alpha \qquad \text{Equation 4}$$

Here it is important to note, the standard laser flash method was designed for dense specimens while measurement of highly porous materials has associated difficulties in defining the applicable specimen thickness L used in Equation 2. To evaluate the effective specimen thickness and density, a three-dimensional high resolution optical profiler Micro Photonics was used to measure the real surface topology (Fig.1). Based on these measurements taken from both sides of specimen, the effective thickness L_{ef} and density were determined and these data were used in Equations 2 and 3 to calculate diffusivity and heat capacity. The laser flash tests were performed from 200C (392F) to 1200C (2192F) at the intervals of 200°C (392°F). Three runs of each type of sample were conducted and the average values are reported in the results.

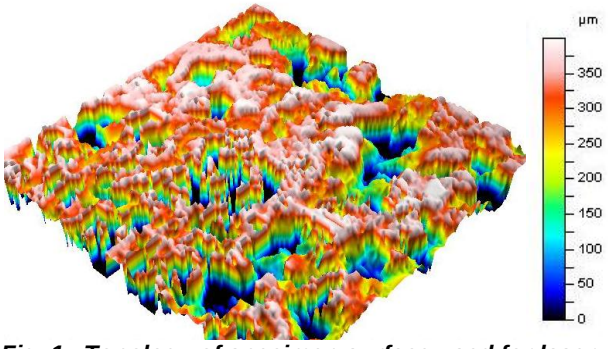

Fig. 1. Topology of specimen surface used for laser flash test is shown.

Densities of the samples were measured before and after laser flash testing by Archimedes method[15] and He pycnometer. These results were used for calculation of bulk density, open porosity (accessible to water), total porosity and closed porosity. In addition, the effective density for laser flash method was calculated based on average specimen thickness using optical profiler.

EXPERIMENTAL COOLING CURVES AND INVERSE MODELING

The shells to be studied were produced by an industrial steel investment casting facility. The shells were built around extruded rigid (blue) expandable polystyrene (EPS) rectangular shape pattern of dimensions 76.2 mm (3 in.) wide by 76.2 mm (3 in.) tall by 25.4 mm (1 in.) thick which was attached to a ceramic pouring cup (Fig. 2). The pattern was carefully chemically dissolved by acetone to avoid crack formation in the shells and then the shells were fired at 850C (1562F) for 1 hr. The shells were allowed to cool down to room temperature prior to pouring. The shells were then entirely wrapped with 12.7 mm (0.5 in.) thick insulating wool (generically made of aluminosilicate fiber), Durablanket S (8 pcf), to thermally isolate the shell and limit the influence of the external cooling environment. The shell was then poured with pure nickel at an initial pouring temperature of 1513C (2755.4F). Properties of pure nickel taken from FACTSAGE[16] database and are given in Table 1.

In order to provide the experimental cooling curves for the "inverse method" procedure, thermocouples were placed at two locations: inside the casting and near the outer surface of the shell (Fig. 2). The cooling curve within the casting was measured with a type S thermocouple in a 2 mm (0.08 in.) diameter quartz sheath. This thermocouple was located 38 mm (1.5 in.) from the bottom of the casting and along the mid-plane of the casting. The shell cooling curve was measured using a K-type thermocouple located at the same height as the casting thermocouple but 1 mm (0.04 in.) inside the outer surface of the mold shell. The K-type thermocouple was bonded in place in the shell with seal coat slurry. A 24-bit data acquisition system was used to collect the data.

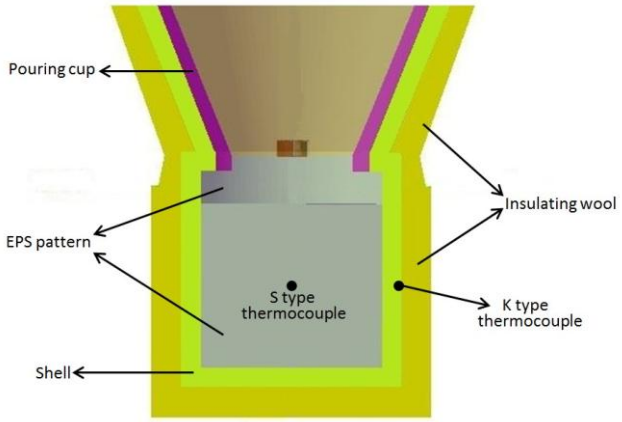

Fig. 2. Schematic of pattern and ceramic investment casting shell mold is illustrated.

For this experimental condition, three types of boundaries needed to be considered. At the first boundary between the casting and the shell, interface heat transfer coefficient (HTC_1) was chosen as 3500 W/m^2K based on published experimental data.[17] This large value of HTC_1 indicated that tight thermal contact taking place between the solidified casting and the shell. It was also assumed that tight thermal contact takes place at the second boundary between the shell and insulating wool. Thus an estimate of HTC_2 = 1000W/m^2K at the interface was used as sufficient to provide negligible thermal impedance relative to the shell and insulating wool layers, as typically recommended by the software producer. Finally, the external HTC_3 between insulating wool and environment was optimized by inverse modeling.

Then multiple iterations of CFD modeling were performed while varying thermal properties of the shell and insulating wool to fit the experimental and calculated curves during solidification. In addition, the temperature dependent external heat transfer coefficient HTC_3 between the insulating wool and environment was also adjusted.

The heat capacities and thermal conductivity of the shell and insulating wool as well as external heat transfer coefficient HTC_3 are the main parameters that influence the temperature curves of the casting and the shell. Preliminary modeling showed that solidification time and the coordinates of the point that the shell at highest temperature shell mainly influenced by heat capacity and thermal conductivity. For higher C_p of the shell, more heat is needed to heat up the shell to a certain temperature, therefore the solidification time will be shorter. Higher K of the shell will allow the heat of the melt to flow through the shell more quickly and then radiate to the air, which also shortens the solidification time and increases the maximal temperature of the shell. Modeling also showed that external heat transfer coefficient HTC_3 mainly affected the shell and casting cooling rates after solidification was completed (Fig. 3).

Table 1. Properties of Pure Nickel Used for Inverse Modeling

Cp, J/g		Latent heat, j/g	T_s, ^{0}C	Density, g/cm^3		K, W/mK	
Solid	Liquid			Solid	Liquid	Solid	Liquid
$(1.62*10^{-4})XT,^0C+0.427$	0.734	279.9	1455	7.9	7.8	80	60

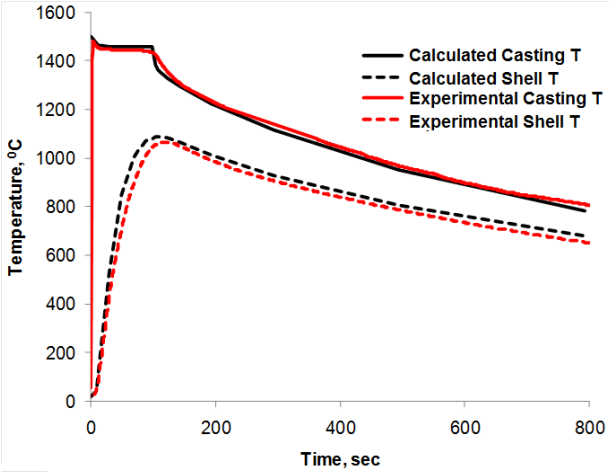

Fig. 3. This graph shows the inverse calculated thermal curves after optimization was fitted to experimentally obtained results.

RESULTS AND DISCUSSIONS

SHELL STRUCTURE AND DENSITY

Because the shell compositions and structures both play important roles in shell thermal properties, microstructure of industrial ceramic shells was evaluated by using the Scanning Electron Microscope (SEM) and the Energy-Dispersive X-ray spectroscopy (EDX) (Fig. 4). The industrial foundry shell had one prime coat made from fused silica and zircon flours with approximately 0.37 mm (1.46 in.) thickness. Five backup coats with total 7 mm (0.28 in.) thickness made from fused silica flour and fused silica stucco and one fused silica flour seal coat (Table 2).

Table 2. Components of Industrial Shells

	Prime	Backup	Seal
Components	Zircon	Fused silica	Fused silica slurry
Thickness, mm	0.4	7	0.1

The structure of the shell is illustrated in Fig. 4. The prime coat had a high density while the next adjacent stucco layer had a high level of small size (10-50 µm) pores. The subsequent stucco layers were built with large particle sizes and had less overall porosity while the individual pores had larger sizes (100-400 µm) and were located randomly. In some cases, these large pores were interconnected to each other.

Porosity of the shells is influenced by processing parameters (slurry viscosity, stucco application method) and stucco size distribution. Combination of viscosity and stucco size is essential for porosity development.[1] For example, finer stucco with a wider size distribution will reduce the porosity of the shell if the slurry has very low viscosity. By comparison, higher viscosity slurry which cannot penetrate into a previously built stucco layer resulted in high overall porosity level with a small individual pore size. Increasing the stucco particle size and slurry viscosity in back up layers results in larger pore sizes while overall porosity will depend on the ratio of these parameters. For example, Figs. 4b and 4c illustrate different levels of penetration of slurry into the previous stucco layer. Better fluidity of slurry with lower viscosity will make the slurry penetrate into the narrow gap between large stucco particles.

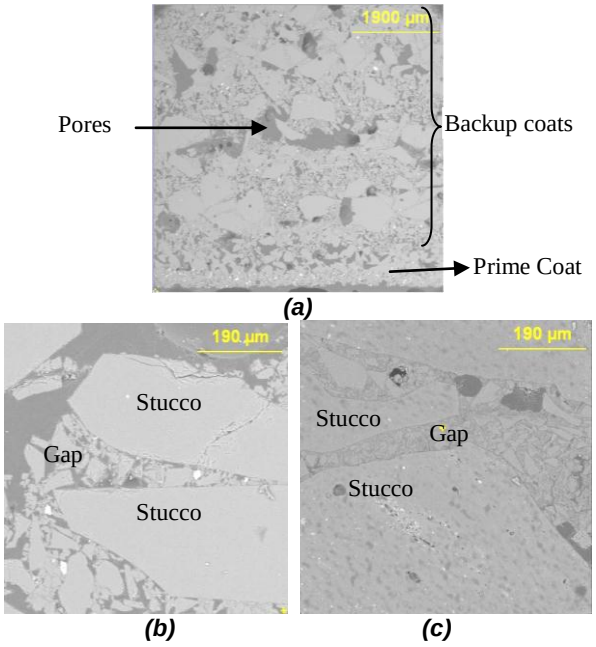

Fig. 4. These photmicrogtaphs show SEM microstructures of industrial foundry shell: (a) prime coats located at the bottom; (b) examples of limited and (c)completely filled gap between stucco particles.

For evaluation of shell density, whole pieces of the shell containing all layers were examined as a first step. Table 3 shows overall bulk density and open porosity accessible for water obtained from Archimedes method. This test provided an average density of whole shell. In addition, theoretical density of a shell specimen after crushing to 100 mesh was obtained from He-pycnometer. In this case,

Table 3. Density and Porosity of Ceramic Shells (Overall Specimen)

Bulk density, g/cm3	Density from pycnometer, g/cm3		Open porosity, %	Closed porosity, %	Total porosity, %
	Whole shell	Crushed shell			
1.64	2.27	2.41	21.7	10.0	31.7

the effect of internal closed porosity was eliminated because He-gas has no restriction for penetration into small size pores when compared to water during testing by Archimedes method. Then the total porosity and closed porosity were calculated from these tests.

The total level of porosity as determined by pycnometer was high (31.7%) with major part of open pores (21.7%) accessible by water from both sides of the specimen during Archimedes testing. The data were obtained at room temperature for the shell fired at 850C (1562F) for 1 hr. To take into account the temperature effect, the known value of thermal expansion $(0.4*10^{-6}/K^{-1})$[18] was used for correction of high temperature densities.

Defined bulk density was used in the "inverse method" because this method assumes heat flux going through the whole shell. In inverse calculation, the real porous material was considered as non-permeable solid media with an average bulk density. By comparison, in the laser flash method, laser energy is absorbed directly by the external front surface and an average infrared temperature response was also measured on porous rare surface. In the case of laser flash measurement, the effective thickness of a specimen as defined from three-dimensional optical profiler was used for calculation of density and heat diffusivity (Equations 2 through 4).

The laser flash method can be used for measurement of local shell properties, in particular, prime coats and back up coats, separately. To determine the local properties of the shell, two-mm thick disks were machined from both prime coat (inner) and back up coats (outer) of the shell. The local densities evaluated by different methods are given in Table 4.

Table 4. Density and Porosity of Inner (Prime Coat) and Outer (Backup Coat) Layers of the Shell

Location	Archimedes and Pycnometer Methods			Optical profiler
	Bulk Density, g/cm^3	Apparent Specific Gravity, g/cm^3	Open Porosity, %	Effective Density, g/cm^3
Inner	1.50	2.15	30.18	1.59
Outer	1.61	2.22	27.67	1.78

It was observed that density of the inner specimen containing prime coat and 1~2 backup coats had lower density and higher porosity than that from outer layers of the shell, which are backup coats. This difference followed from the microstructures of these specimens (Fig. 4a). In particular, the inner specimen comprised prime coat and first back up layer made with fine stucco. High viscosity of the applied slurry did not allow it to penetrate among fine stucco particles, resulting in development of high macroporosity. The outer specimen from backup coats had larger size pores but with lower overall level of porosity and higher density.

COMPARISON AMONG DIFFERENT METHODS

Specific heat capacity and thermal conductivity of the inner and outer specimens from the ceramic shell as measured by modified laser flash method are shown in Fig. 5. It is obvious that the specimens taken from each side have similar C_p values over the temperature range tested, while the thermal conductivity (K) of the inner specimen is lower than that outer specimen due to higher porosity.

Two sets of thermal properties data were obtained by "inverse method": (i) for insulating wool (Table 5) and (ii) for ceramic shells (Fig. 6). These data characterize the thermal properties of overall shell structure.

Table 5. Insulating Wool Thermal Properties

	***T*, °C**	**300**	**600**	**900**	**1200**
Calculated	K, W/mK	0.06	0.15	0.25	0.32
	C_p, J/kgK	950	1050	1080	1100
Manufacture provided	K, W/mK	0.08	0.18	0.30	-
	C_p, J/kgK	1130 J/kgK at 1093 °C			

The high temperature thermal properties of the ceramic shell which were experimentally obtained with laser flash method were compared to those obtained from inverse modeling of the casting process data as well as to theoretically predicted values from the properties of pure refractory materials,[16, 19] considering the porosity effect using Equation 1. Figure 7 shows the specific heat capacity of the shell obtained from different methods, as well as C_p values of the pure refractory materials at different temperatures.

The heat capacity values of pure materials and the shell substantially increased with increasing temperature. Temperature dependent specific heat capacities of the shell from experimental measurement and inverse calculation results are larger than values predicted by the mixture rule (20wt% zircon + 80wt% silica) for pure crystalline materials. This is possibly due to endothermic reactions among shell components or phase

transformation within the amorphous silica at high temperature. The rate of these reactions will affect the measured C_p values. For example, the "inverse method" showed a larger C_p value than laser flash because this method is associated with more instantaneous measurements of a property including latent heat associated with phase changes as compared to the partially thermally stabilized specimen condition used in the laser flash test. To prove the unsteady state effects on C_p values, C_p measured by laser flash and C_p from inverse calculation results were compared with the previously published[4] C_p values of a silica ceramic shell obtained with DSC, which provided an even larger C_p at high temperature due to longer exposure time. DSC indicated a lower value at low temperature due to phase reconstitutions upon heating, while the "inverse method" actually gave the properties of shell during cooling, where some of phase reconstitutions have already occurred during pouring.

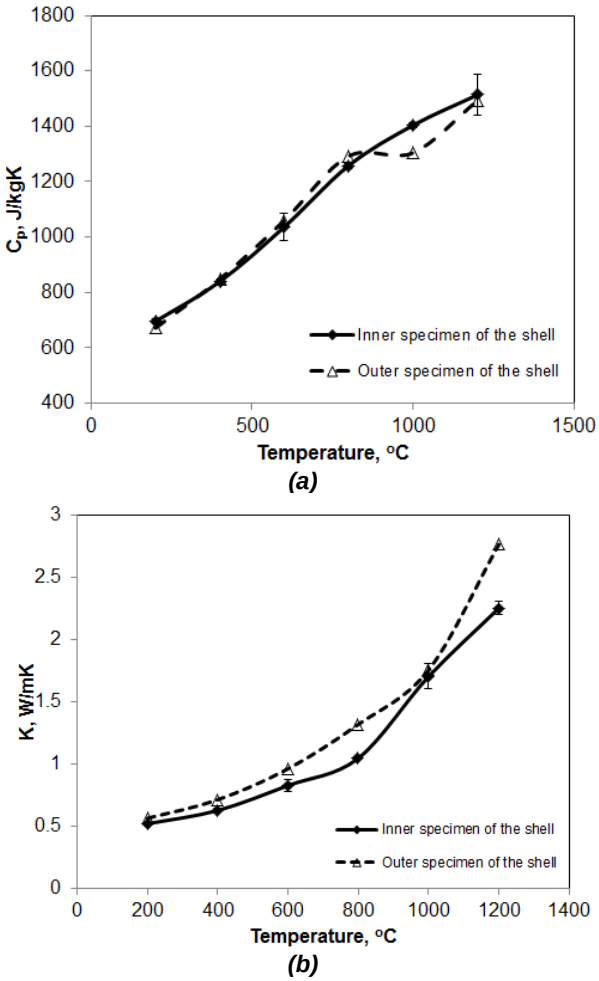

Fig. 5. The graphs show (a) specific heat capacity and (b) thermal conductivity of inner and outer specimens of the shell obtained by the modified laser flash method.

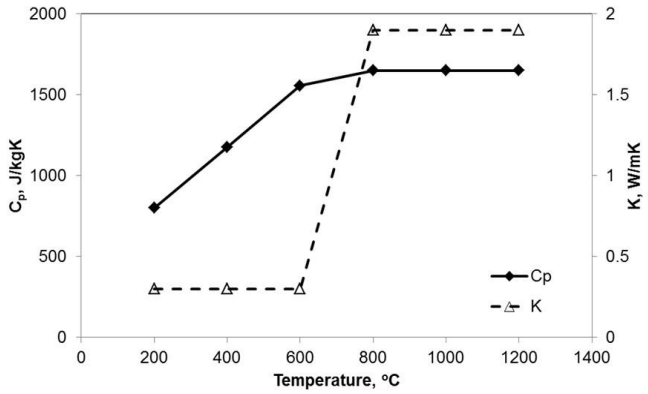

Fig. 6. Thermal properties are obtained from Magmasoft inverse modeling.

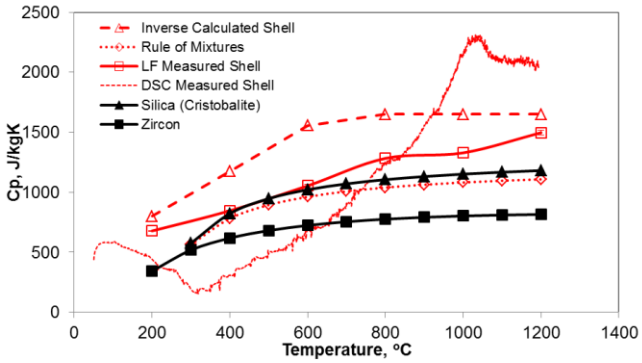

Fig. 7. Graph shows the comparison of specific heat capacity (C_p) of industrial foundry shells, obtained from different methods.

Figure 8 shows the thermal conductivity of the shell obtained from different methods, as well as *K* values of the pure refractory materials at different temperatures. Thermal conductivity of pure zircon decreases with increasing temperature because increasing lattice vibration energy and crystal imperfections such as boundaries and dislocations will interrupt with phonons causing phonon scattering. However, *K* values of pure silica (cristobalite) increase with increasing temperature due to activation of photon thermal conductivity (thermal radiation in transparent media).

Because the main component of the specific shell studied is fused silica with a colloidal silica (amorphous) binder matrix, the measured thermal conductivity has a similar trend to pure silica (cristobalite). Also, the shells had lower thermal conductivity at room temperature and higher values at high temperature when compared to pure silica. The theoretically predicted values of properties, based on properties of the pure material components using models that also consider porosity effects (Equation 1), are significantly lower than those obtained from other experimental/modeling methods. Therefore, the theoretical prediction from pure materials using the rule of mixtures and porosity cannot be recommended for estimation of thermal conductivity of ceramic shells.

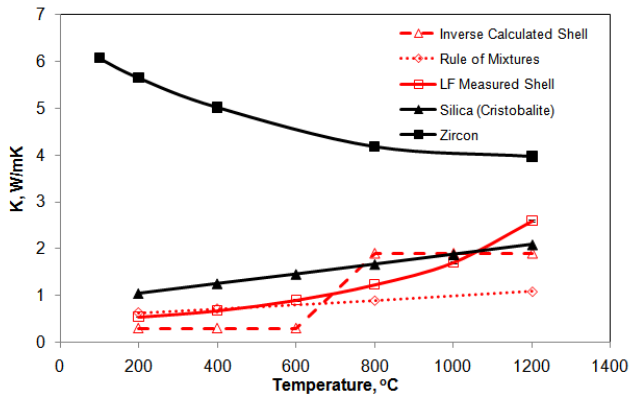

Fig. 8. Graph shows the comparison of coefficient of thermal conductivity (K) of shell obtained by different methods and pure materials.

The results obtained from modified laser flash method gives the best correspondence to date with inverse calculation results. In addition, laser flash method can be used to measure the local thermal properties of the layered porous investment shell, for example, prime coat and different back up layers. These measurements could be used to design molds with desired thermal properties by combining multi-layer ceramic stucco structure with different thermal properties for each layer. For this multi-layer ceramic stucco structure, the effective heat resistance (R, K/W) in steady state heat transfer can be estimated as for a sandwich type structure:

$$R = \sum_i \frac{L_i}{SK_i} \qquad \text{Equation 5}$$

where: K_i is coefficient of thermal conductivity of layer i with thickness L_i and S is surface area.

Variations in K value and layer thickness will provide the possibility to intensify or slow casting solidification depending on desired situation.

CONCLUSION

A modified procedure to correct laser flash results for porous specimens has been developed. The thermal properties including specific heat capacity and thermal conductivity of industrial shell materials were measured using modified laser flash and compared to published data obtained from DSC.[4] Instrumental measurements were compared to inverse modeling results using experimentally obtained cooling curves from the casting process. The influences of the shell composition and microstructure were discussed and thermal properties were compared to pure refractory materials with theoretical correction from specimen porosity.

Discrepancies among C_P from different methods were discussed. It can be concluded that the "inverse method" provided more realistic average C_P values for investment casting process when compare to instant values obtained from laser flash method. Moreover, in terms of total enthalpy, DSC measured the heat of reactions having a higher degree of completion than the extents of reaction which occur in the real casting process.

The theoretically predicted values, based on properties of pure material while taking the effect of porosity into consideration, are not recommended for prediction of thermal conductivity of ceramic shells. Laser flash with effective specimen thickness correction is recommended to measure the local thermal properties of the porous investment shell. The "inverse method" has been used to confirm overall shell heat conductivity. The database obtained can be used to improve the precision of solidification shrinkage prediction in investment casting modeling.

ACKNOWLEDGMENT

The authors would like to thank U.S. Army Benet Labs for funding this research under contract number W15QKN-07-2-0004. The authors appreciate the assistance of Dr. Jeffrey Smith and Todd Sander for laser flash analysis. The authors wish to acknowledge support of participating foundries for providing shell samples for this study and Metsch Refractories Inc. for supplying pouring cups. We would also like to thank Eric Bohannan for his help running DSC and Matthew Thompson and Gregory Harrington for operating Laser Flash Equipment. The authors wish to recognize the assistance of Tom Towey and Bradley Bromet for sample and heat preparation.

REFERENCES

1. Kline, D.M., Lekakh, S.N., Richards, V.L., Chandrashekhara, K., Chen, J., "Stucco Size Comparison and Simulated Pressure Loading of Investment Casting Shells," *AFS Transactions*, vol. 117, pp. 341-353 (2009).
2. Ding, S., Zeng, Y., Jiang, D., "Gas Permeability Behavior of Mullite-Bonded Porous Silicon Carbide Ceramics," *J Mater Sci*, vol. 42, pp. 7171-7175 (2007).
3. Isobe, T., "Gas Permeability and Mechanical Properties of Porous Alumina Ceramics with Unidirectional Aligned Pores," *Journal of the European Ceramic Society*, vol. 27, pp. 53-59 (2007).
4. Mahimkar, C., Richards, V. L., Lekakh, S.N., "High Temperature Thermo-Physical Properties of Ceramic Shell," *57th Annual Technical Meeting: Investment Casting Institute* (2010).
5. Zivcova, Z., Gregorova, E., Pabst, W., Smith, D., Michot, A., Poulier, C., "Thermal Conductivity of Porous Alumina Ceramics Prepared Using Starch as a Pore-Forming Agent," *Journal of the European Ceramic Society*, vol. 29, pp. 347–353 (2009).

6. Kline, D.M., Lekakh, S.N., Richards, V.L., "Improving Investment Casting Mold Permeability Using Graphite Particles," *AFS Transactions*, vol. 118, pp. 159-165 (2010).
7. Jones, S., Yuan, C., Blackburn, S., "Fundamental Study on Microstructure and Physical Properties of Fluidized Bed and Rainfall Sanding Ceramic Shells," *Materials Science and Technology*, vol. 23, no.6 , pp. 706-714 (2007).
8. Hart, G "The Nomenclature of Silica," *American Mineralogist*, vol. 12, pp. 383-395 (1927).
9. Connolly, S., Jones, S., Marquis, P.M., "Specific Heat of Investment Casting Shells," *BICTA Issue 44*, pp. 23-26 (2004).
10. Garcia, E., Osendi, M.I., Miranzo, P., "Thermal Diffusivity of Porous Cordierite Ceramic Burners," *Journal of Applied Physics*, vol. 92, no. 5, pp. 2346-2349 (2002).
11. Huang, H., Berry, J.T., Zheng, X.Z., Piwonka, T.S., "Thermal Conductivity of Investment Casting Ceramics", *37th Annual Technical Meeting : Investment Casting Institute* (1989).
12. Majchrzak, E., "Identification of Cast Steel Latent Heat by Means of Gradient Method," *Int. J. Computational Materials Science and Surface Engineering*, vol. 1, no. 5, pp.555-570 (2007).
Carlson, K.D., Beckermann, C., "Development of Thermo-physical Property Datasets, Benchmark Niyama Results, and A Simulation Qualification Procedure," *Proceeding of the 64th SFSA Technical and Operating Conference*, Paper No. 5.5 (2010).
13. Sabau, A.S., Viswanathan, S., "Thermo-Physical Properties of Zircon and Fused Silica Based Shells for Investment Casting," *AFS Transactions*, vol. 112, pp. 649-661 (2004).
14. Shinzato, K., Baba, T., "A Laser Flash Apparatus for Thermal Conductivity and Specific Heat Capacity Measurements," *Journal of Thermal Analysis and Calorimetry*, vol. 64, page 413-422 (2001).
15. "Standard Test Methods for Apparent Porosity, Water Absorption, Apparent Specific Gravity and Bulk Density of Burned Refractory Brick and Shapes by Boiling Water," *ASTM C 20-00*.
16. FactSage(TM) 6.2.
17. Woolley, J.W., Woodbury, K.A., "The Interfacial Heat Transfer Coefficient of Metal Castings-A Literature Review," *AFS Transactions*, vol. 0.75, pp. 1-18 (2007).
18. Lekakh, S.N., Kline, D.M., Chandrashekhara, K., Chen, J., Richards, V.L., "Process Parameters Study for Net-Shape Steel Casting," *Shape Casting: The 3rd International Symposium, TMS* (2009).
19. James, F., Alexander, W., *CRC Practical Handbook of Materials Selection*, pp. 404-4.